IPNO DRE 98-01

LIGHT PARTICLES EMITTED WITH VERY FORWARD QUASI-PROJECTILES AND THE MECHANISM IN THE FRAGMENTATION OF 44 MeV/a.m.u. ^{40}Ar

Particules légères en coincidence avec les quasi-projectiles détectés à 0° et le mécanisme de fragmentation pour des ^{40}Ar à 44 MeV/u.m.a.

P.Roussel, Ch.O.Bacri, V.Borrel, E.Kashy[1], C.Stéphan, L. Tassan-Got, D.Beaumel, M.Bernas, F. Clapier, M.Mirea[2].

1) *Michigan State University, East Lansing, U.S.A.*

2) *Institute of Atomic Physics, Bucharest, Romania*

LIGHT PARTICLES EMITTED WITH VERY FORWARD QUASI-PROJECTILES AND THE MECHANISM IN THE FRAGMENTATION OF 44 MeV/a.m.u. ^{40}Ar *

P.Roussel, Ch.O.Bacri, V.Borrel, E.Kashy†, C.Stéphan, L. Tassan-Got,
D.Beaumel, M.Bernas, F. Clapier, M.Mirea‡
Institut de Physique nucléaire
Université Paris XI, CNRS, IN2P3
91406 Orsay Cedex FRANCE

Abstract

The mechanism of projectile fragmentation in the Fermi-energy region has been investigated for fragments emitted in the incident beam direction by detecting fast protons and neutrons evaporated by the projectile-like fragments. The proton coincidence rate is shown to increase with fragment velocity loss. This increase is also correlated to the decrease of the fragment yield, with the coincident rate doubling when the yield decreases by a factor of 10. The coincidence rate is found to be also proportional to the fragment mass loss for fragments with the beam velocity. A two-step mechanism is sketched out to interpret these results. For fragments with the beam velocity, the projectile nucleon removal is equally shared between a first fast step and the second evaporative step, while for fragments at the tenth of the maximum yield, the nucleons are removed by evaporation. Finally, the experimental observation that the most probable velocity for forward fragments is very close to that of the beam may be the result of a strong forward/backward momentum asymmetry in a Goldhaber-type analysis.

Keywords NUCLEAR REACTIONS. Projectile fragmentation. ^{58,64}Ni, Al, Au(^{40}Ar,X,n,p), Θ_X=0°, measured (X,n,p) coincidence rate. Study of peripheral reaction mechanism.

Pacs 24.10.-i,25.60.Gc,2570.-z,25.70.Lm,25.70.Mn,25.70.Pq

*Experiment performed at the GANIL facility

†Michigan State University, East Lansing, U.S.A.

‡Institute of Atomic Physics, Bucharest, Romania

1 Introduction.

Projectile fragmentation in the Fermi-energy region is a complex mechanism which can be however described as a two-step process. A fast initial step leads to the elimination of several nucleons through ablation or pre-equilibrium emission or intra-nuclear cascades. Many other processes can actually contribute to this initial step, including direct transfer or multi-transfer reactions, or nucleon or cluster exchange or even charge exchange.The excited body which results has a decreased velocity which, on the average, does not change as it emits particles through evaporation leading to the observed final fragment. This is the slow second step of the reaction.

This study focuses specifically on fragments detected in a very forward direction thus minimizing the transverse energy. The more abundant fragments were chosen. The very forward angle of observation insured a high differential cross section which leads to a high counting rate. In this angular region, the most probable fragment velocity is much closer to the beam velocity than at the grazing angle[1] and, as shown in Fig.1, much closer than expected from simple models. The present coincidence measurements were performed to explore the behavior of the light particles emitted together with these forward fragments.

As in a previous experiment[1], a 44 MeV/a.m.u. ^{40}Ar beam was used and the targets chosen range from ^{27}Al to ^{197}Au. In the intermediate mass region, targets of two isotopes ^{58}Ni and ^{64}Ni were used in order to investigate the role of the target neutron excess for a better understanding of the mechanism.

2 Experimental setting

The detection system was specifically designed for fragments near 0^o and has been described in detail elsewhere (Ref[2],[3]). A double magnetic spectrometer was used in the telescopic (parallel to point global tuning) mode. A mosaic of ΔE-E telescopes identified fragments and a PPAC in the focal plane yielded their positions which were converted into highly accurate emission angles. This accuracy of about 1.5 mr. in the reaction angle is illustrated in Fig.2 with the ^{40}Ar elastic scattering from protons in a polyethylene target.

In order to improve statistics, results from several detectors were summed for the data presented here, with an average detection angle of $\simeq$9.6 mr(0.55^o). Note that the average fragment angle tends to be even smaller due to the angular distribution.

Neutrons and protons were the main light particles detected in coincidence with the

projectile fragments. A set of five cells filled with NE213 liquid scintillator was used. A 3mm thick steel absorber followed by a thin plastic scintillator was placed in front of each cell. For coincident events with the plastic scintillator signal in veto, a threshold at $\simeq$ 1 MeVe (electron equivalent) was required to identify neutron events. During a test experiment using the NE213 γ/neutron light discrimination method, this criterium was observed to reliably select neutrons in coincident events. When the thin plastic scintillator was used as a trigger, charged particles were selected, most of them being protons with an energy threshold at $\simeq$ 50MeV due to the steel absorber.

The geometry of the counter array (Fig. 3) was designed to enhance the detection of nucleons emitted by evaporation from the projectile fragment. The angular aperture of the cells were between 5 and 25^0. A kinematics calculation shows that, for a heavy fragment at the beam velocity, evaporated nucleons are emitted in the forward direction within a 15^0 cone up to 3 MeV kinetic energy, within a 25^0 cone up to 7.5 MeV. At 11 MeV kinetic energy, still half of these nucleons are emitted within this 25^0 cone. Thus the array had a low efficiency for the nucleons evaporated from the target, since they are spread over the entire 4π space, so that less than 5% of them are emitted within this angular domain. Nucleons emitted in the fast initial first step of the mechanism were not expected to interfere significantly as they have been predicted[4] to peak between 20 and 30^0 for a heavier projectile (^{84}Kr) at a higher energy (200 MeV/u) and were expected here at still larger angles.

Attention was focused on fragments with masses A_F from approximately 15 to 35 for which the two step mechanism is more likely to apply. For heavier fragments, direct reactions play a dominant role and for lighter fragments the mixture of mechanisms becomes more complex while the collision is more central and violent. The coincidence rate between these fragments and the neutrons and protons was examined versus v/v_0, the ratio of the fragment velocity to that of the beam. Events with only one nucleon detected in coincidence dominate and were selected.

3 Experimental results

Fig.4 shows a clear dependence of the coincidence rate on the (final) fragment velocity. The same is true nearly over the whole range of masses and targets, though the dependence which is rather weak for low A fragments is found much stronger when the fragment mass gets closer to that of the projectile. Different $N - Z$ (neutron excess) values are presented but as will be shown below it is the fragment mass which is the lead-

ing factor for the slope of the variation. A similar behaviour was observed for neutrons though with less statistics.

Either a linear or an exponential gives acceptable fits to the data over the whole range of targets and A_F values. Each has only two parameters. The first parameter is the coincidence rate C_0 at the beam velocity, that is near the peak fragment yield (for fragments detected close to the beam direction). The second parameter, $C_{1/10}$, is the coincidence rate where the fragment yield is down by a factor of 10 from the peak yield, on the low velocity side of the distribution. It occurs when fragments have a velocity which we will refer to as $v_{1/10}$ the plot of which is found in Fig.1. This choice is guided by the observed similarity between the changes of slope of the coincidence rate and the fragment yield versus the fragment mass A_F. For practical reasons, the coincidence rate $C_{1/10}$ was determined at the velocity $v_{1/10}$ evaluated for the ^{58}Ni target when analyzing data for all targets.

In order to obtain C_0 and $C_{1/10}$, interpolations or extrapolations were performed. As noted before, both a linear and an exponential fit could be used. At beam velocity, the deduced values C_0 do not significantly depend on this choice (see Fig.4). But at $v_{1/10}$, the differences may become significant, in particular for fragments with low A_F values and $N = Z$ for which the extrapolation is extended further away from the experimental points. For these fragments, the exponential fit amplifies the consequences of experimental errors and consequently, it is the linear fit which has been chosen for all the fragments.

Different N - Z values around that of the most abundant fragments (see Fig.8 of Ref[1]) were chosen. The selected A_F ranges go respectively from 12 to 28, from 11 to 35, from 18 to 40 and 27 to 41 for $N - Z$=0,1,2 and 3 (the latter, being too close to the beam's $N - Z$ value, have not been included in the global fits).

We first examine the value C_0 of the coincident rate between light particles and the forward fragments detected at the beam velocity and its variation with A_F for the different targets.

Results for protons (Fig.5) have smaller error bars and are more reliable than for neutrons (Fig.6). In both cases, the coincidence rate decreases when the fragment mass increases and gets close to zero as the fragment mass approaches that of the projectile. For protons, C_0 varies linearly with the mass A_F of the detected fragment over the whole range of masses so that, C_0 is proportional to the difference between A_F and the mass of the projectile (40). Note that fits do not depend much on the value of $N - Z$.

For neutrons, if a linear variation is to be found, it does not extend up to the projectile

mass (see Fig.6)

This is more precisely examined with a two-parameter linear fit (table I) which exhibits the value of the coincidence rate in the middle of the A_F range (A=25), and the value of A_F for which the coincidence rate decreases to zero.

In the middle of the A_F range (A_F=25) the values of C_0 are very similar for Al and the Ni targets. Even with gold target, for protons, the value differs only by 25% while for neutrons, all the values fall within ±7%.

For protons, the extrapolated A-value for zero coincidence rate is actually found close to 40 and a fit (not shown) which sets the value at 40 remains quite acceptable. It reflects the above mentioned proportionality between the coincidence rate and the mass difference between the fragment and the projectile. This is not found for neutrons where the extrapolated A_F value for ^{64}Ni is considerably larger than for ^{58}Ni indicating a significant role for the target neutron excess which is also seen when comparing on Fig.6 the results for the ^{64}Ni target with that of ^{58}Ni.

Since all events are clearly associated with neutrons or with protons and not with undifferentiated nucleons, we plotted the coincidence rate versus 2N for neutrons and versus 2P for protons, instead of the fragment mass A, and compared the crossing points to 36 (twice the projectile proton number) and 44 (twice the projectile neutron number) respectively. This resulted into a slight improvement for protons but worsened that for neutron, especially for $N - Z$=3.

Let us now look at $C_{1/10}$ the coincidence rate for fragments when the yield is down to one tenth of its peak i.e. at the velocity $v_{1/10}$. The proton case (Fig.7) is very similar to that for C_0 at v_0 except for low A_F values. For neutrons (Fig.8), the similarity is less clear as the variation of $C_{1/10}$ with A_F has flattened.
Following for $C_{1/10}$ a similar procedure as for C_0, a two-parameter linear fit leads to table II.

In comparing table I and II, a noticeable effect is seen. The coincidence rate values for A_F=25 at the reduced speed (table II) are found to be approximately twice as large as those for fragments at the beam velocity (table I). The ratio $R = C_{1/10}/C_0$ has values of 2.28, 1.96, 2.00, 2.15, for protons and 1.96, 1.62, 1.53, 1.68, for neutrons, respectively for ^{27}Al, ^{58}Ni, ^{64}Ni, ^{197}Au. The extrapolated A_F values are close enough so that the value of R$\simeq$ 2 for A_F=25 remains valid for a wide range of A_F values. It indicates, with better evidence for protons, that for any given final fragment, the velocity decrease which leads to an attenuation of the yield by a factor of ten corresponds to a doubling in the coincidence rate. This is also equivalent to a statement that the slopes of the exponential

describing the two velocity-related distributions are proportional (with opposite sign).

Note also that for low A_F values, a strong odd-even effect is present (Fig.7) which was not observed (Fig.5) for the coincidence rate at the beam velocity. It means that a significant odd-even effect is present in the slope of the coincidence rate versus the velocity. The slow fragment with an even mass is accompanied with a larger number of light particles than the odd one.

4 DISCUSSION

We will first focus attention on protons where the results exhibit more clarity, then on neutrons, and finally on the puzzling problem of the very small velocity shift of the projectile fragments with respect to the beam.

PROTONS

For an observed fragment of mass A_F, the total loss of mass $\Delta = (A_P - A_F)$ is shared as $N_1 = (1-\alpha)\Delta$ and $N_2 = \alpha\Delta$ between the two steps of the mechanism, where α is the fraction which goes into evaporation. It has been implicitly assumed that, if nucleon transfer occurs, it does so, on the average, either from projectile to target or conversely with equal probabilities, and it does not affect the fragment mass. Of course, α a priori depends on both the final fragment mass and on its velocity, $\alpha(v_F, A_F)$ which will be labeled α_0 for fragments at the beam velocity and as $\alpha_{1/10}$ for fragments at the velocity $v_{1/10}$ for which the fragment production yield is reduced to its tenth.

We further assume that the evaporated nucleons N_2 are detected with a small and *constant* efficiency ϵ while nucleons emitted in the initial first step are not detected at all. Both these assumptions are to a large degree justified by the properties of the experimental setup as described earlier.

For an event in the mass range of interest observed at the beam velocity, the number of nucleon detected is:

$$n_2^0 = \epsilon N_2^0 = \epsilon\alpha_0(A_P - A_F)$$

Similarly for the same fragment with the reduced velocity $v_{1/10}$:

$$n_2^{1/10} = \epsilon N_2^{1/10} = \epsilon\alpha_{1/10}(A_P - A_F) = \epsilon R\alpha_0(A_P - A_F)$$

where, as previously defined, R has an experimental value of $\simeq 2.$ for the range of mass fragment considered.

But as a consequence of the assumption that transfers do not, on the average, change the projectile mass, $\alpha_{1/10} = R\alpha_0$ cannot exceed 1 and α_0 has an experimental upper

bound $\alpha_{0\,max}$ with:

$$\alpha_0 < \alpha_{0\,max} = 1/R \simeq 0.5$$

Therefore, for fragments at the beam velocity, which is close to the most probable velocity, no more than half the nucleon removal comes from evaporation.

The upper bound ($\alpha_{0\,max} \simeq 0.5$) does depend on the choice of the reduced velocity (here $v_{1/10}$) to which we have ascribed the maximum of the coincidence rate. A choice of a smaller velocity would lead to a smaller value for $\alpha_{0\,max}$. Here, the velocity $v_{1/10}$ where the yield is 1/10 the peak yield was chosen. It is roughly within the range of velocity from v_0 to $v_{1/10}$ that the variation of the coincidence rate has been parameterized and moreover, it is also believed that at still lower velocity, the assumed two step mechanism is no longer applicable. So evaluated, $\alpha_{0\,max}$ is found independent of the fragment mass A_F and of its $N - Z$ value. it is also found independent of the target. But α_0 could indeed depend upon A_F. However it is found (again, with more evidence for protons and not so much for neutrons) that this is not the case since n_2^0, and consequently N_2^0, has been found proportional to $A_P - A_F$. The common value of α_0 has an upper bound of $\alpha_{0\,max}$, but can it be determined better within the limits of 0. and $\simeq 0.5$. Surprisingly enough, the knowledge of α_0, together with the constraint that the coincidence rate is doubled at velocity $v_{1/10}$ enables one to parameterize all the two-step events. It becomes for instance possible on the one hand, to calculate the number of evaporated nucleons, once the number of abraded nucleons and the velocity change of the first step are given or on the other hand, to calculate the nucleon removal in each of the two steps leading to a final fragment when its mass and its velocity are given. The variation of $v_{1/10}$ with A_F is based on the data shown on Fig.6 of Ref.[1] and is

$v_{1/10} = 1. - W_E(A_F)$ where $W_E(A_F)$ the width at 1/10 of the peak yield was parameterized as:

$$W_E(A_F) = 0.117 exp(-0.1(A_F - 25)) + 0.002 \quad (1)$$

Using this expression, we are now able to deduce the consequences of different choices for the parameter α_0 , and to visualize them in the $A \times v/v_0$ plane.

Such a description will offer a representation of the whole scheme of the mechanism. It is done on Fig.9 in the case of $\alpha_0 = \alpha_{0\,max} \simeq 0.5$ and also, for a comparison purpose, for a much smaller value α_0 =0.2. Different values of the final fragment mass A_F are represented as well as different values of the intermediate (hot) fragment mass A_I.

As expected for $\alpha = \alpha_{0\,max} \simeq 0.5$, and as depicted on the upper left figure, events with no first step nucleon removal (pure friction events) populate final fragments along the line corresponding to the variation of $v_{1/10}$ with A_F (see eq.1) i.e. events at the tenth

of the peak yield. And there is no way towards final fragments with a lower velocity. More generally for this value of α_0, low yield events come from small first step removal n_1 and different dissipations leading to different values for n_2 and finally to different A_F. In contrast, for high-yield (high-velocity) events, the total mass loss Δ, n_1 and n_2 are proportional and hence highly correlated.

As also seen on the right hand half of Fig.9, another quantity which strongly depends on α_0 is the ratio of the number of evaporated nucleons during the second step to the fractional velocity change of the projectile (or of the intermediate fragment). It can be shown that this ratio is proportional to the ratio α_0 /(1-α_0). This calculated slope varies from $\simeq$1 nucleon per 1% change in dv/v when α_0 =.5 to $\simeq$0.25 nucleon when α_0 =0.2. But considering energy transfer, we now discuss why $\alpha_0 \simeq 0.5$ is more realistic.

The slowing down of the projectile is equivalent to an energy decrease of 35 MeV per 1% change in dv/v. Assuming that this energy transfer is shared equally between the target and the projectile and assuming that an average energy (binding plus kinetic) of 13 MeV is needed for the removal (e.g. evaporation) of one nucleon would lead to a slope of 1.3 nucleon per 1% change in dv/v which is slightly greater than is its empirically deduced maximum value $\alpha_0 \simeq .5$.

On the other hand, the creation in the projectile of n_1 nucleon holes during the first step, when assumed with no friction at all, should lead to an excitation of $\sim 13 n_1$ MeV[5] and it should then be followed by the evaporation of the same number of nucleons. From more realistic evaluations[6], one would actually expect a greater number (up to twice as many) and consequently α_0 would be expected to have a value even larger than 0.5. It seems then that α_0 is somehow constrained to have a value close to its empirical maximum at $\alpha_{0\,max} \simeq 0$ .5, and it is this value which will be kept as an experimental result and be used below.

As regards the role of the target, the similarity of the proton results for the two isotopes of nickel though they differ by as much as 6 neutrons is striking. For both isotopes, results are like those for aluminum and support the expectation that emission of nucleons by the projectile is selectively detected. However, for the gold target, the coincidence rate is weakly but definitely lower at the beam velocity as well as at $v_{1/10}$ the reduced speed. For gold, the use of the nickel distribution width could be at the origin of an observed difference but for aluminum, this cannot be the case. It is tempting to evoke a size effect, the large gold target interfering with the light particle emission from the projectile.

NEUTRONS

At beam velocity (Fig.6), and for the ^{58}Ni and Al targets, the neutron coincidence rate behaves like that for protons. It is not the case for the ^{64}Ni target where the rate rises steeply for fragments close to the projectile, but then flattens to a much smaller slope than for ^{58}Ni. Note that the neutron detection not only differs from the proton detection due to the nature of the detected nucleon but also because of the energy threshold which is 50MeV for protons and much lower at $\simeq$ 4MeV for neutrons. Thus while no protons evaporated by the target are detected, some neutrons from the target can be detected and might be occurring significantly for the neutron rich ^{64}Ni target.

At the reduced velocity, neutron results differ significantly from those for protons. Since neutrons from the target are partially detected they may affect results for the highly damped collisions expected at reduced velocity for all targets. In any case, the two-step process as parameterized for protons cannot be established from the neutron results.

It must be noted however that in an experiment measuring the *target* neutron multiplicity with the same argon projectile on a gold target at incident energies from 27 to 44 MeV/a.m.u., an increase of that multiplicity also was observed for decreasing *projectile* fragment velocities and the average neutron multiplicity was found proportional to the *projectile* mass loss.[7],[8]

THE ENERGY BALANCE AND THE MECHANISM

We have now to come back to the main question concerning forward fragments. *Why such a small damping for the final most probable fragment velocity.* We recall now that for those events (see Fig1), there is an excess of energy of $\simeq$6MeV/n, as compared to the limiting cases of a pure friction evaporation model with no kinetic energy for the evaporated nucleons, or a pure fragmentation model with cold residues.[1]

Reviewing the basis of this apparent excess of kinetic energy, we have:

(i) The observed velocity of the final fragment was taken as that of the projectile fragment before evaporation and could not exceed that of the incident beam.

(ii) The energy transfer from the incident motion to the internal degrees of freedom is equally shared between the projectile and the target in proportion to their mass.

(iii) This internal energy is used for the removal of single nucleons with no kinetic energy, with an average energy cost of $\simeq$9MeV/n.

Note that a change in the models towards a more realistic evaporation (energetic

[1]The difference between the two models is that the evaporated nucleons stay at rest in a cloud around their respective originating source in the former but are all together allowed to interact within a fire ball in the latter.

nucleons) or fragmentation (hot fragments) will increase the energy mismatch between the observation and the model, leading to the question of the mechanism responsible for the needed energy recovering.

This mismatch was seen to some degree in earlier measurements at the grazing angle (Fig.1) which lie just at the limit of no kinetic energy for nucleon evaporation or of cold residues for the fire-ball fragmentation scheme. Because of success in analyzing high incident energy results [9], [10], and in analyzing the high energy part of the momentum distribution[11],[12],[13], the cold residues model was accepted until it was demonstrated, with heavier projectiles and on the basis of the observed average N/Z value of fragments, that evaporation with a much higher excitation energy was required [14],[15], [4] (see also the review article[16]). But still, the mismatch remained.

Note that for forward fragments at $v_{1/10}$, events fit reasonably a pure friction mechanism with 4 to 9 MeV for the evaporated nucleon kinetic energy. But these events are ten times less probable than those near v_0. For events near v_0, the above question remains crucial and can be stated as follows: since half the nucleon removal comes from nucleon evaporation in the second step of the mechanism, (with the associated energy consumption), not only must the first step not consume energy from the incident projectile kinetic energy, but it must also provide a source of energy in order to compensate for evaporation.

To provide this energy, one may consider modifying or even dropping the above assumptions. As regards (iii) and as mentioned in Ref[1], the required energy can be found if all the emission consists of clusters or alpha particles instead of nucleons. But this has not been established for forward fragments and it is known to be incorrect at the grazing angle where nucleon emission dominates over cluster emission. As regards (ii), it is clearly violated for the transfer of one nucleon which heats the acceptor much more than the donor. And it would be even more so for a massive transfer. In any case, asymmetric transfer would compound the problem for forward fragments.

It seems finally that abandoning assumption (i) may provide a solution to this energy problem, considering the major role of the nucleon Fermi motion as evidenced by Goldhaber model and confirmed by experiment.

Let us first quote Goldhaber[17].

> *Suppose that A nucleons are assembled with zero net three momentum,* $\mathbf{p}_A$*=0.* If K of these nucleons chosen at random should go off together as a single fragment, *what would be the mean square total momentum* $\mathbf{p}_K^2$*. The A nucleons have mean square momentum* $< p^2 >$*.*

One finds that $< p_K^2 >= \sigma^2 = K(A-K)/(A-2) < p^2 >$

with $\sigma_0^2 =< p^2 >= 3P_F^2/5$ when P_F is the Fermi momentum of the nucleon.

It gives a value σ_0=100 MeV/c. From initial high energy experiments where all the fragments were detected together, a slightly smaller value σ_0=90 MeV/c was found. In fitting grazing angle measurements σ_0 has a value of 85MeV/c, and a value σ_0=67 MeV/c fits the current very small angle results. Note that a Gaussian distribution (as predicted for the p_K distribution in the Goldhaber model) factorizes in its components and that its width remains unchanged whether all the fragments are detected or only a narrow angular part of them. The forward fragment distribution should have had the theoretical width whereas it is found to be 67% .

Consider a situation where the nucleons emitted by the fragments observed are not *chosen at random* and they do not *go off together as a single fragment* as assumed in the Goldhaber scheme, but rather they are separated during the collision. For the observation of forward fragments, the internal momentum $\mathbf{p}_K$ must be aligned with the laboratory projectile momentum, either with the same direction or with the opposite one. One may then postulate that the separation of the fragment K in the forward direction is more likely than backward. Thus the selection of the forward fragmentation would produce a change in the average velocity which goes from zero to a positive value introducing in this way a violation of hypothesis (i). The fragment velocity is no longer that of the projectile. Furthermore such a selection, the detail of which is unknown, is likely also to produce a change of the shape of the distribution and of its width.

A similar but less drastic selection would apply for grazing angle fragments with a less pronounced forward/backward asymmetry. And even for fragments at any angle, it would be expected that some forward/backward asymmetry remains.

The prediction of a calculation with 4 MeV of kinetic energy alloted to each nucleon removed (see Fig.10) was shifted the equivalent of the half width at tenth of maximum of the theoretical Goldhaber distribution. This shift is represented by the arrows in fig.10. The good match to the data shows that an asymmetry, though rather drastic, could explain the observed effect.

5 CONCLUSION

In the study of very forward projectile fragmentation, a strong correlation between the fragment velocity and the number of detected nucleons has been established with both coincident protons and neutrons. With an experimental apparatus specifically designed

to detect nucleons evaporated by the projectile, the proton results indicate that, for events at the most probable velocity, the nucleon removal is equally shared between the first fast step and the second evaporative step. For a given fragment mass, essential pure friction events are found for velocity at which the yield is one tenth the peak yield. A close relationship has been found between the evolution with the fragment velocity of the yield and of the coincidence rate (the slope of the former being 4 times larger than that of the latter). It suggests that the number of evaporated nucleons is essentially determined once the number of abraded nucleons and the velocity loss are known. Finally a large forward/backward asymmetry in the first step fragmentation has been suggested to explain the observed fragment high velocity.

It should be emphasized that the present results apply for selected events with projectile fragments detected in the very forward angular region. It would be interesting to investigate the fragment angular distribution up to and beyond the grazing angle and also to increase the incident energy to a value where the width due to Fermi motion exceeds that resulting from friction-evaporation.

P. Lelong, L. Petizon, G. Voltolini, are acknowledged for their essential support in the preparation of the experiment. Their role and that of R. Alves-Condé[2] was also very important during the experiment. F. Ameil, F. Jubin and C. Pailhes are acknowledged for their help during the experiment. One of us (E.K.) was supported in part by the U.S. National Science Foundation.

References

[1] Ch.O. Bacri, P. Roussel, V. Borrel, F. Clapier, R. Anne, M Bernas,Y Blumenfeld, H. Gauvin, J. Herault, J.C. Jacmart, F. Pougheon, J.L. Sida, C. Stephan, T. Suomijarvi, L. Tassan-Got, Nucl. Phys. **A555** (1993) 477.

[2] Ch.O. Bacri, PhD Thesis, Orsay, France (1989) IPNO-T-89-09

[3] Ch.O. Bacri and P. Roussel, Nucl. Instr. and Meth. **A300** (1991) 89.

[4] C. Donzaud, L. Tassan-Got, C. Stephan, D. Bachelier, Ch.O. Bacri, R. Bimbot, B. Borderie, J.L. Boyard, F. Clapier, T. Hennino, M.F. Rivet, P, Roussel, D. Bazin, C. Grunberg, D. Disdier, B. Lott, C. Volant, Nucl. Phys. **A593**(1995)503.

[2] Ganil

[5] J.J. Gaimard, K.H. Schmidt, Nucl. Phys. **A531** (1991) 709. and references included

[6] K.H. Schmidt, T. Brohm, H.G. Clerc, M. Dornic, M. Fauerbach, H. Geissel, A. Grewe, E. Hanelt, A. Junghans, A. Magel, W. Morawek, G. Münzenberg, F. Nickel, M. Pfützner, C. Sheidenberger, K. Sümerer, D.J. Vieira, B. Voss, C. Ziegler, Phys. Lett. **B360** (1993) 313

[7] J. Galin, J.L. Charvey, H. Doubre, J. Fréhaut, D. Guerreau, G. Ingold, D. Jacquet, U. Jahnke, D.X. Jiang, B. Lott, C. Magnago, M. Morjean, Y. Patin, J. Pouthas, Y. Pranal and J.L. Uzureau, 26^{th} Bormio winter meeting, Bormio, Italy, January 25-30 1988. Proceedings p.140.

[8] M. Morjean, J. Fréhaut, D. Guerreau, J.L. Charvey, G. Duchêne, H. Doubre, J. Galin, G. Ingold, D. Jacquet, U. Jahnke, D.X. Jiang, B. Lott, C. Magnago, Y. Patin, J. Pouthas, Y. Pranal and J.L. Uzureau, Phys. Lett. **203B** (1988)215.

[9] H.H. Heckman, D.E. Greiner, P.J. Lindstrom and F.S. Bieser, Phys. Rev. Lett. **28** (1972) 926.

[10] Y.P. Viyogi, T.J.M. Symons, P. Doll, D.E. Greiner, H.H. Heckman, D.L. Hendrie, P.J. Lindstrom, J. Mahoney, D.K. Scott, K. Van Bibber, G.D. Westfall, H. Wieman, H.J. Crawford, C. Mc. Parland and C.K. Gelbke, Phys. Rev. Lett. **42** (1979) 33.

[11] V. Borrel, These de 3^{ieme} cycle, Orsay, France (1984) IPNO-T-84-02.

[12] D. Guerreau, V. Borrel, D. Jacquet, J. Galin, B. Gatty, X. Tarrago, Phys. Lett. 131B (1983) 293

[13] F. Rami, J.P. Coffin, G. Guillaume, B. Heusch, P. Wagner, A. Fahli and P. Fintz, Nucl. Phys. A444 (1985) 325

[14] L. Tassan-Got and C. Stéphan, Nucl. Phys. **A 524** (1991) 121.

[15] Tassan-Got L., PhD thesis Orsay, France (1988) IPNO-T-89-02. and Tassan-Got L., XXVI International Winter Meeting on Nuclear Physics Bormio January 25-30, 1988, p323.

[16] B. Borderie, M.F. Rivet and L. Tassan-Got, Ann. Phys. **15** (1990) 287.

[17] A.S. Goldhaber, Phys. Lett. 53B (1974) 306

	protons ^{27}Al, ^{58}Ni, ^{64}Ni, ^{197}Au	neutrons ^{27}Al, ^{58}Ni, ^{64}Ni, ^{197}Au
coincidence rate C_0 for A_F=25 (10^{-1})	0.608, 0.673, 0.625, 0.466	0.276, 0.308, 0.320, 0.279
A-value extrapolated for zero coincidence rate	43.8, 42.0, 43.5, 42.1	48.1, 45.5, 60.1, 51.9

Table I: Results from a linear fit on the variation of the coincidence rate with the fragment mass at the beam velocity (see Fig.5 and Fig.6). The values of the coincidence rate (CR) are given in the middle of the range of interest i.e. A_F=25. The A-value extrapolated for zero coincidence rate (crossing point with the A_F axis) is the second set of parameters.

	protons ^{27}Al, ^{58}Ni, ^{64}Ni, ^{197}Au	neutrons ^{27}Al, ^{58}Ni, ^{64}Ni, ^{197}Au
coincidence rate $C_{1/10}$ for A_F=25 (10^{-1})	1.39, 1.32, 1.25, 1.00	0.54, 0.50, 0.49, 0.47
A-value extrapolated for zero coincidence rate	44.1, 45.9, 45.0, 44.8	50.2, 62.1, 67.7, 55.3

Table II: Results from a linear fit on the variation of the coincidence rate with the fragment mass at the reduced velocity $v_{1/10}$ (see Fig.7 and Fig.8). The values of the coincidence rate (CR) are given in the middle of the range of interest A_F=25. The A_F value for the crossing point with the A_F axis (coincidence rate at zero) is the second set of parameters.

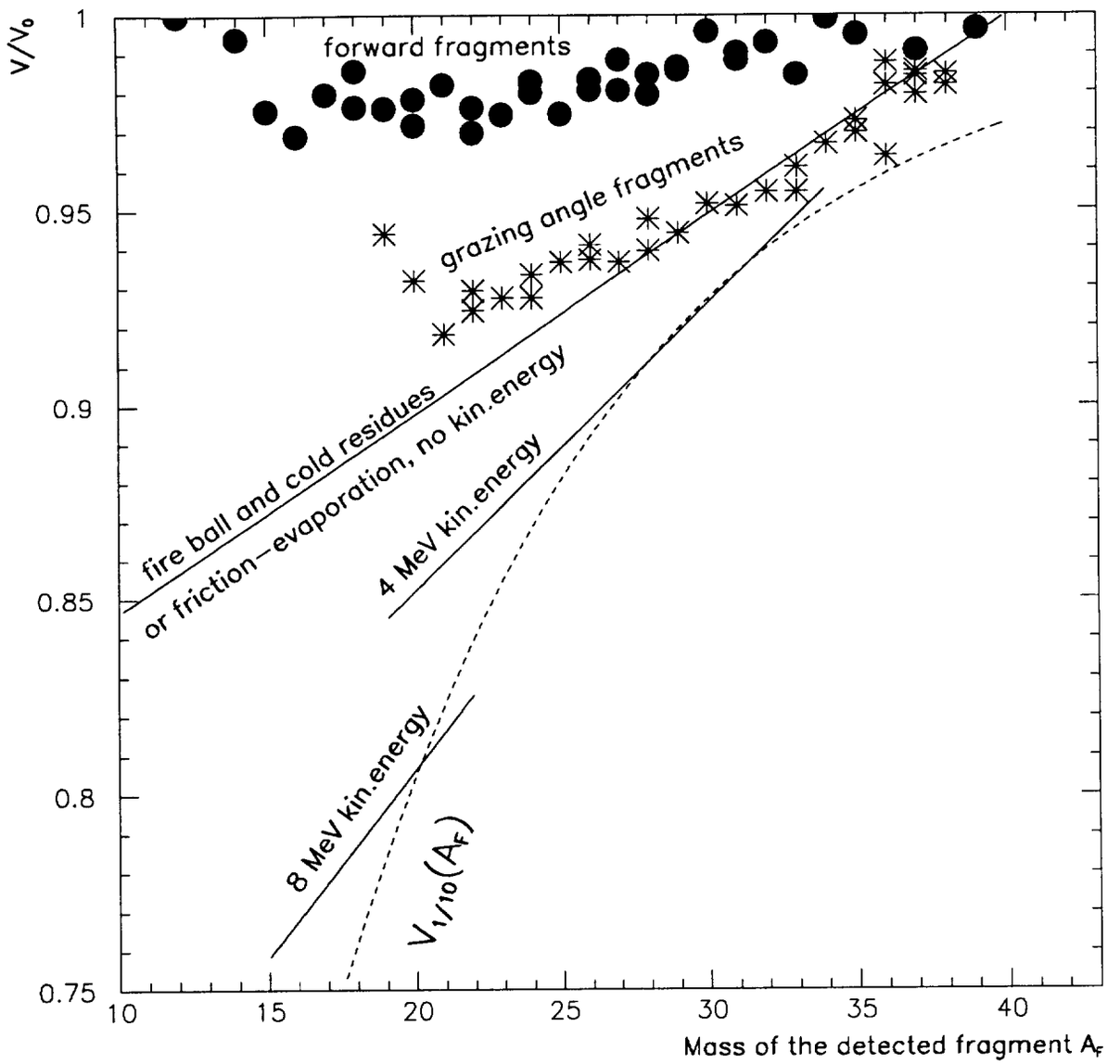

Fig.1 Most probable relative velocity versus the fragment mass A_F for fragments detected in the beam direction (bold points), or at the grazing angle (stars), the data are from Ref.[1]. The most abundant fragments for the case of the ^{58}Ni target are presented. The prediction of a friction-evaporation model are given (continuous straight lines) with the assumption of an equal sharing of the friction energy between target and projectile and for different values of the evaporated-nucleon average energy, 0, 4 and 8 MeV. With the value 0, it is also the prediction for a fire ball model with cold residues. The dashed line shows the fragment velocity relative to the beam ($v_{1/10}$) for which the forward-fragment yield is 1/10 its peak value (see Ref.[1]).

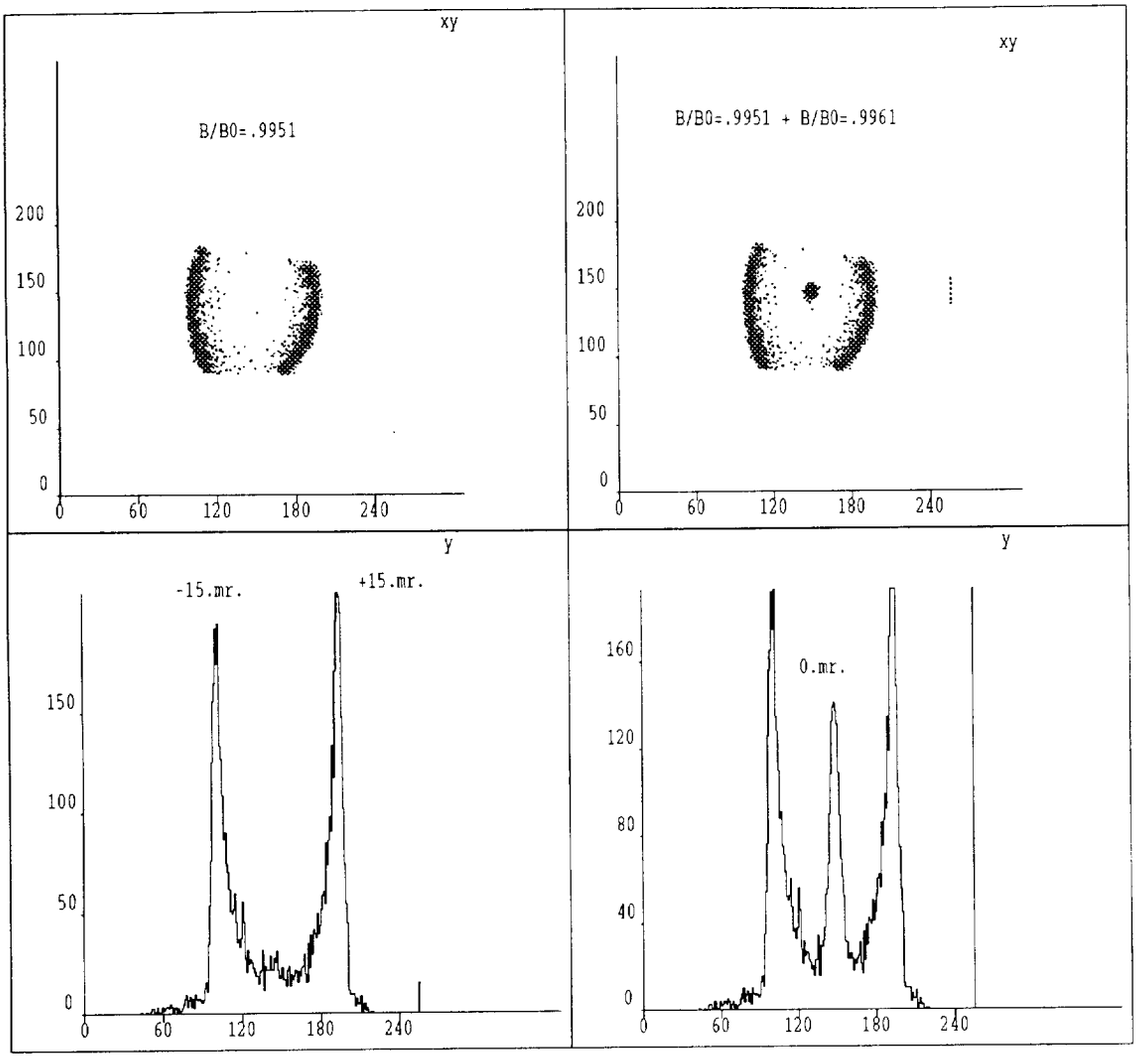

Fig.2 Calibration of the spectrometer telescopic mode using the elastic scattering of the incoming ^{40}Ar beam on a proton (polypropylene) target. The focal lengths correspond to dispersions of 0.18 and 0.10 cm/mr in the X and Y directions. The top half of the figure shows the scatter plot of X, Y positions in the focal plane. The bottom half is the Y spectrum for a centered narrow band in X. On the left part of the figure the spectrometer magnetic rigidity is set to B/B_0=.9951± 0.0005 of that of the beam, that is, for elastic scattering at $\theta \simeq 15mr$. On the right part, a short exposure is added at $B/B_0 = .9961 \pm 0.00025$ so that the low energy tail of the incident beam shows up giving a signature for θ=0.

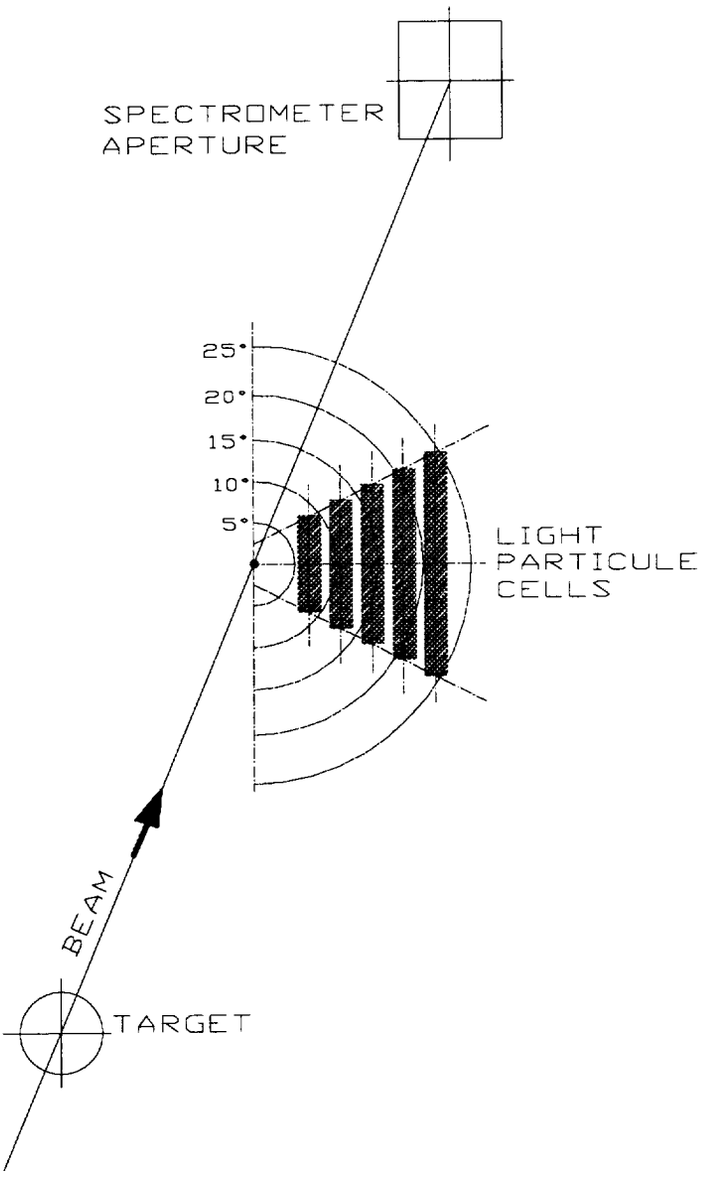

Fig.3 Scheme of the light particle detectors. The beam direction is perpendicular to the plane of the figure and angles from the target with respect to the beam are labeled.

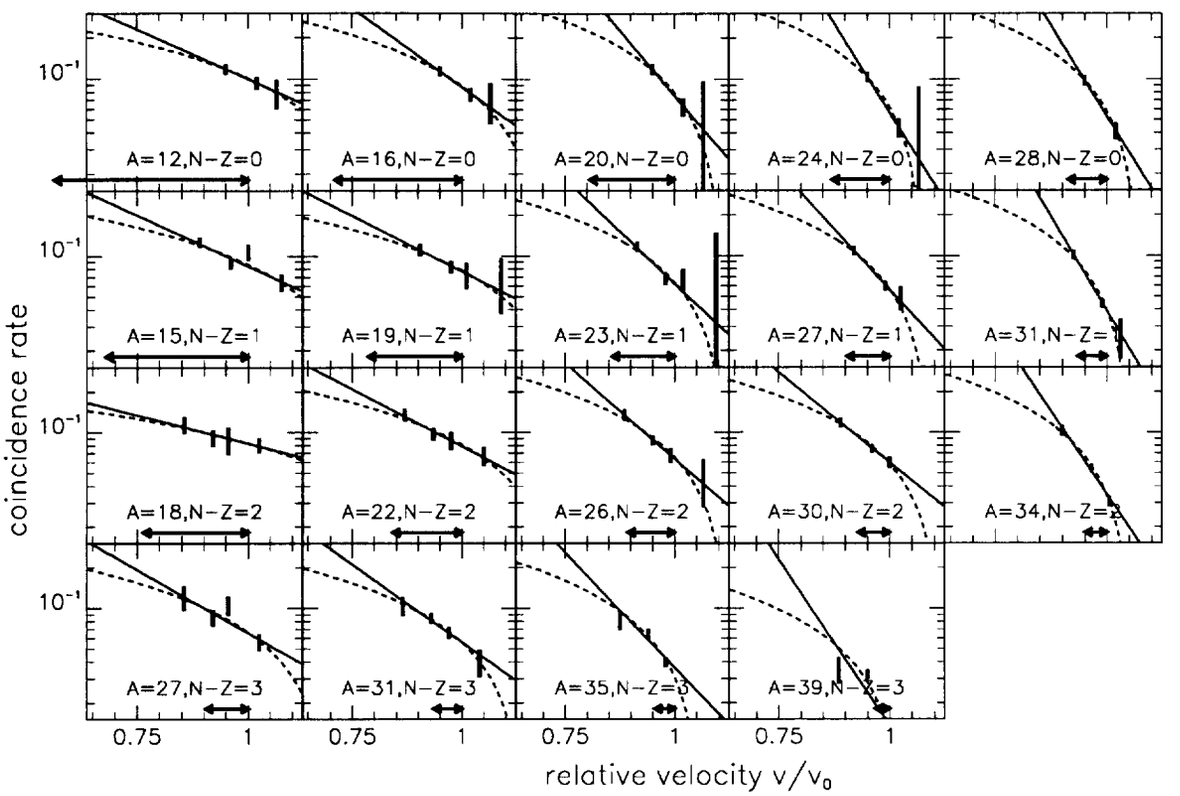

Fig.4 Variation of the proton coincidence rate versus the relative fragment velocity for a ^{64}Ni target. Both a linear (dashed line) and an exponential (full line) fit are shown. The horizontal arrow indicates the width of the fragment production yield: The arrow starts at the beam velocity, close to the peak fragment yield. The yield is down by a factor 10 at the left end of the arrow, i.e., at v= $v_{1/10}$ (see Fig.1).

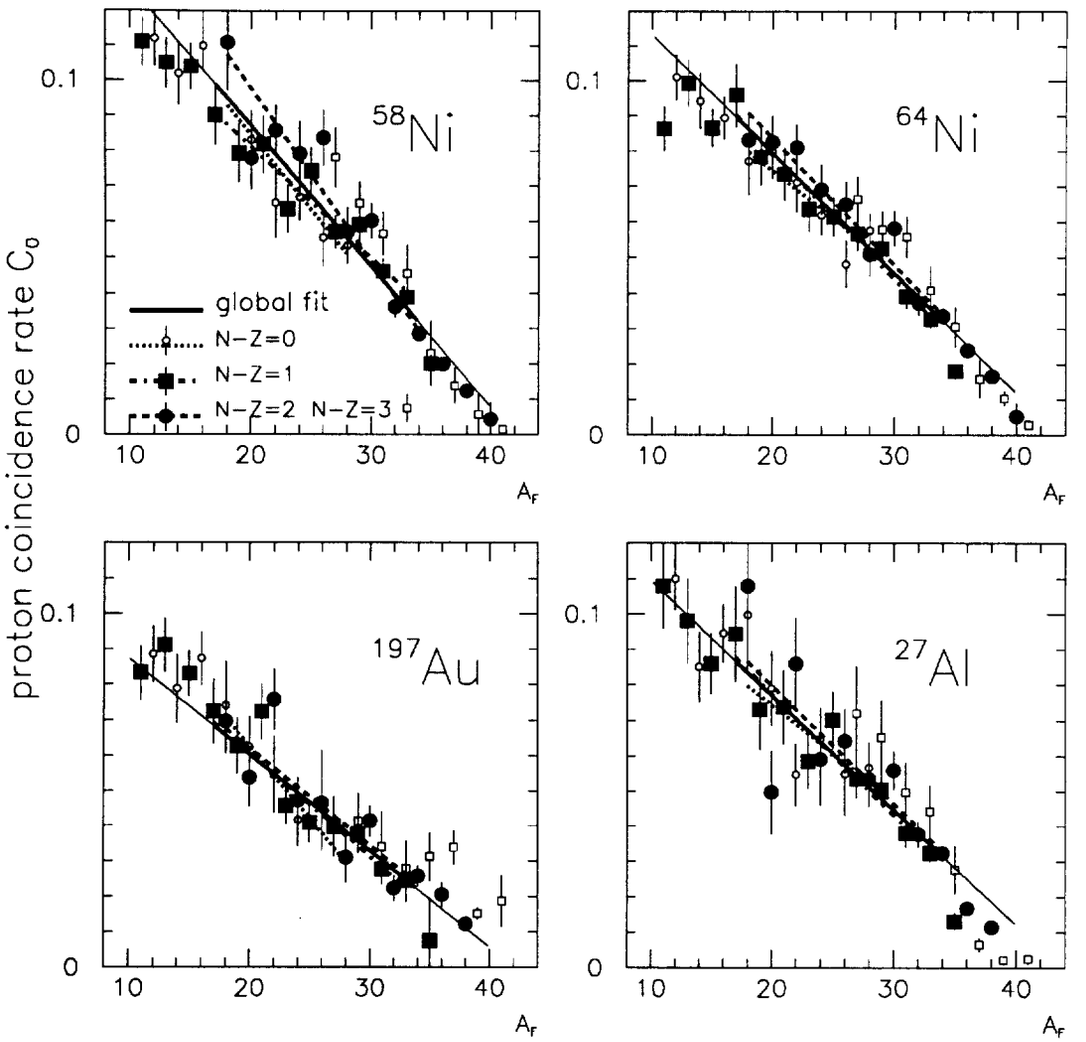

Fig.5 Proton coincidence rate C_0 for fragments at the beam velocity versus the mass of the final fragment. Small symbols are for $N - Z=0$ (even masses) or $N - Z=3$ (odd masses); larger symbols (for larger yields) are for $N - Z=1$ (odd masses) and $N - Z=2$ (even masses). The mass range for separated and global fits are indicated by the thick lines. The global fit is prolongated by a thin line. The value $N - Z=3$ is not fitted and not included in the global fit.

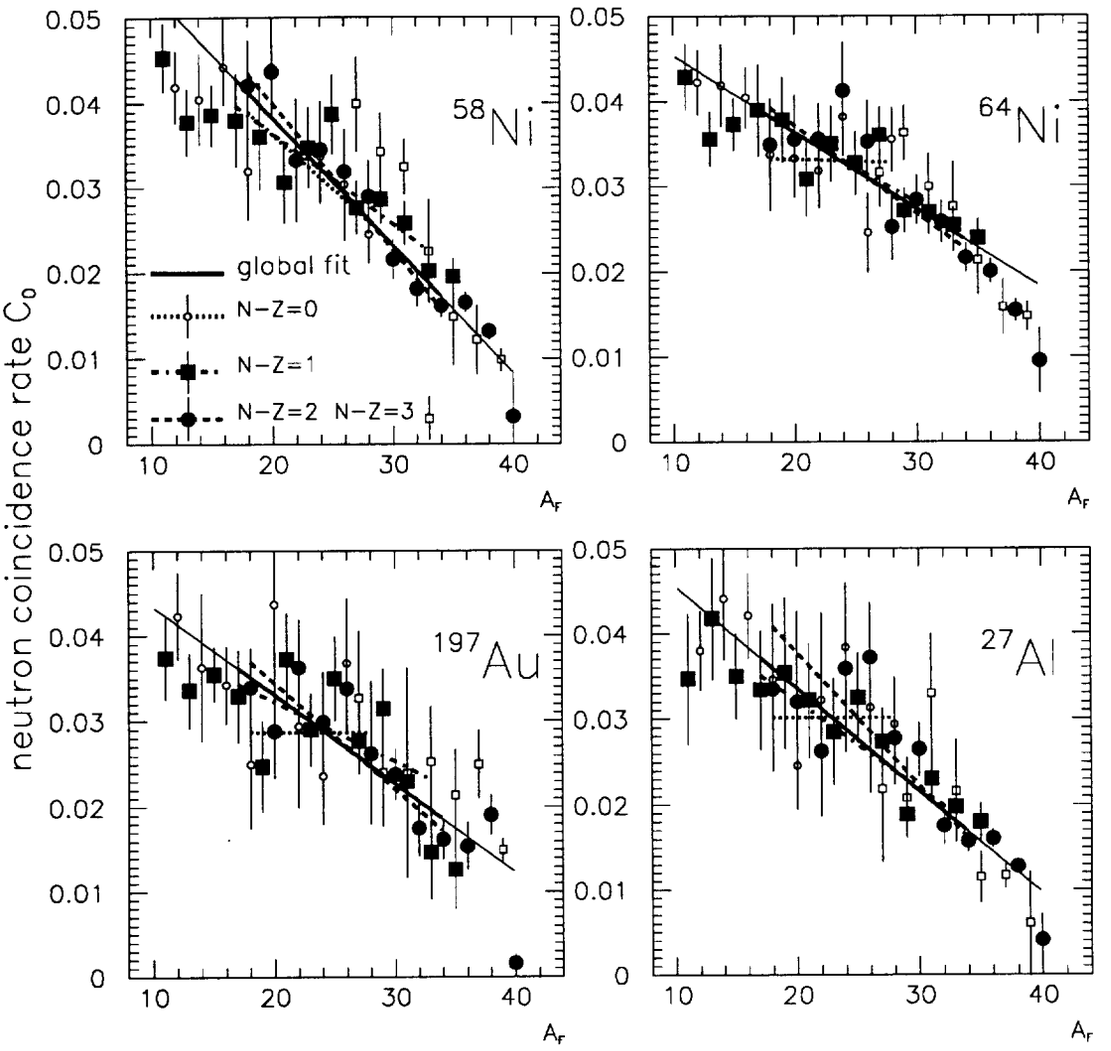

Fig.6 Neutron coincidence rate C_0 for fragments at the beam velocity versus the mass of the final fragment. See caption of Fig.5.

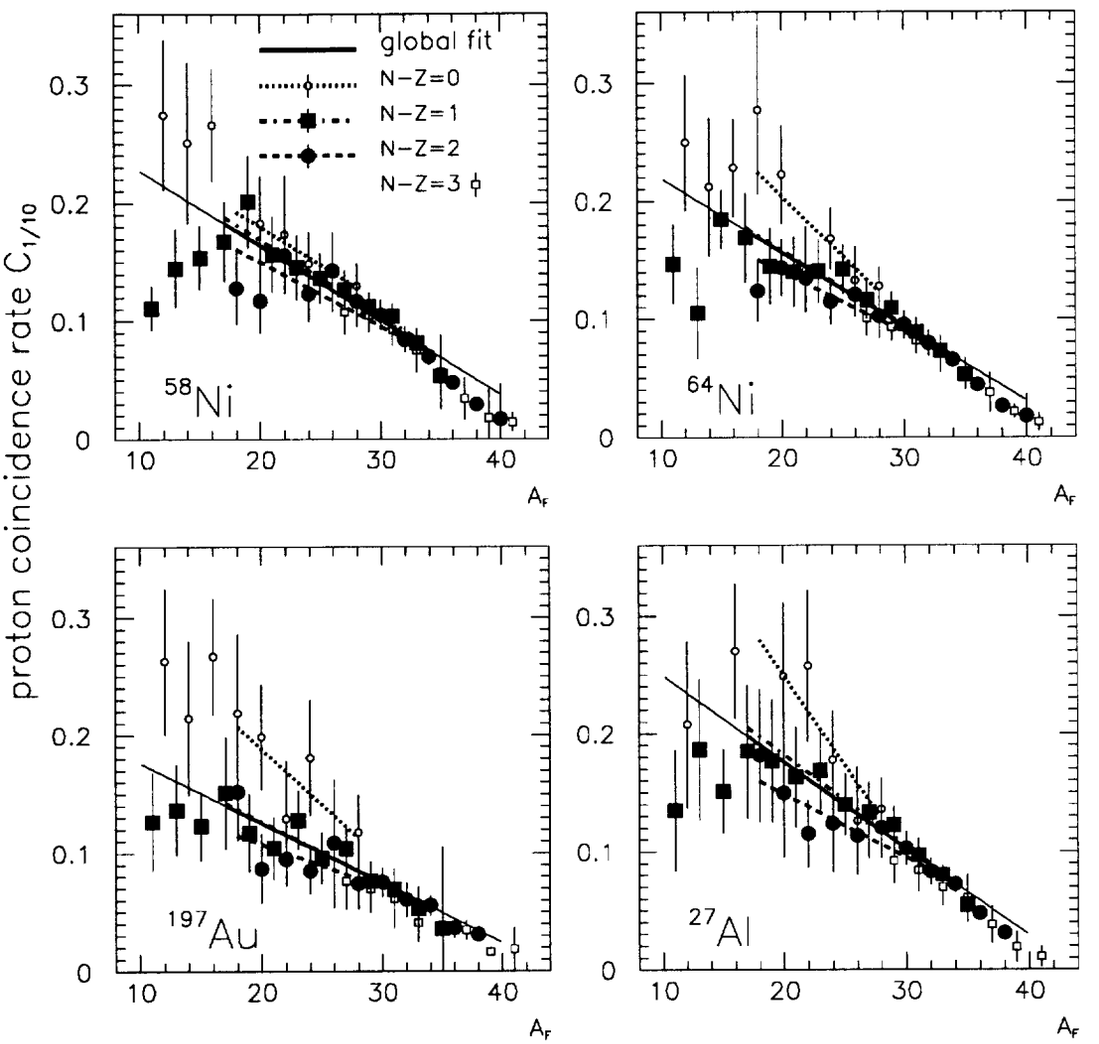

Fig.7 Proton coincidence rate $C_{1/10}$ versus the mass of the final fragment for fragments at the reduced velocity $v_{1/10}$ where the fragment yield is down by a factor of 10. See caption of Fig.5.

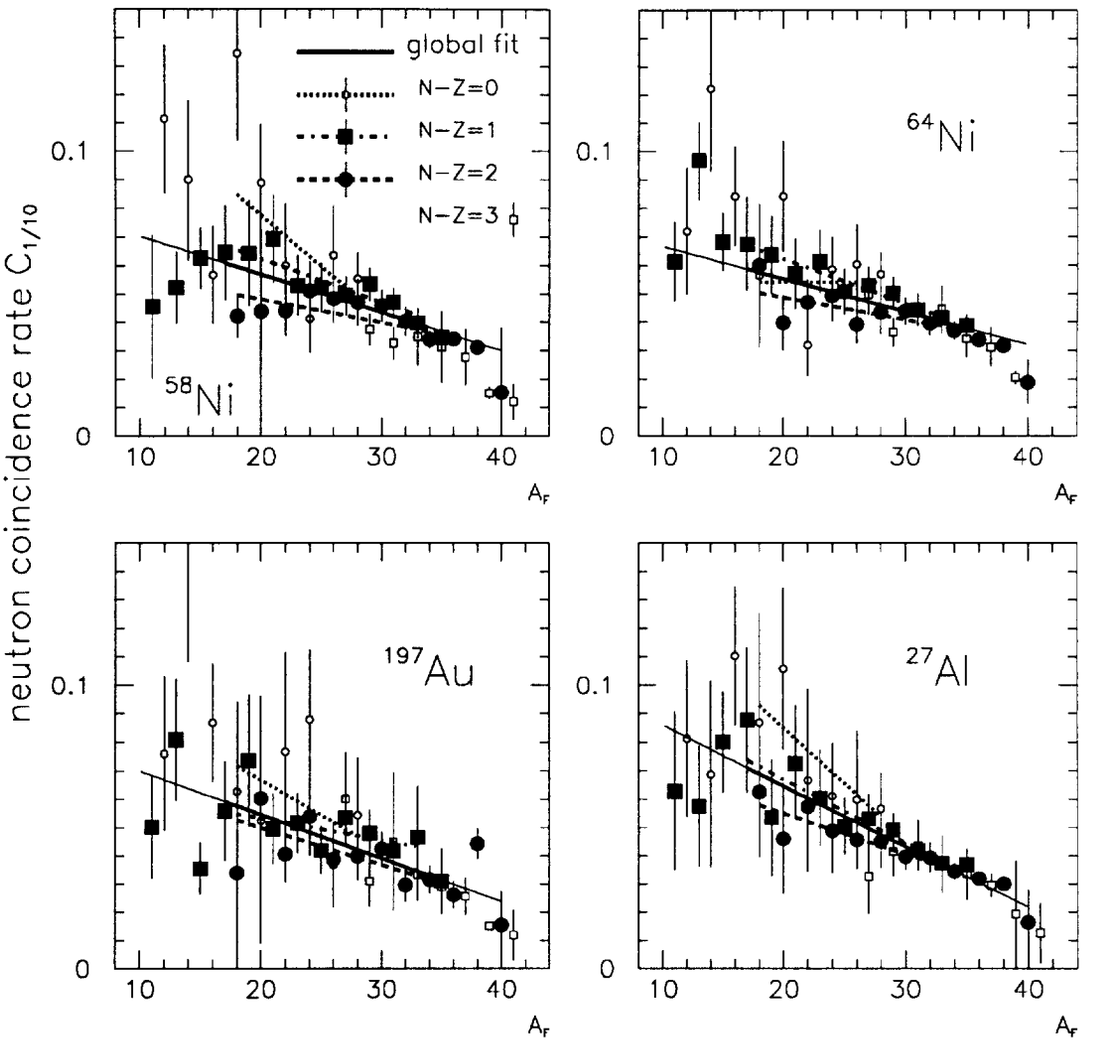

Fig.8 Neutron coincidence rate $C_{1/10}$ versus the mass of the final fragment for fragments at the reduced velocity $v_{1/10}$ where the fragment yield is down by a factor of 10. See caption of Fig.5.

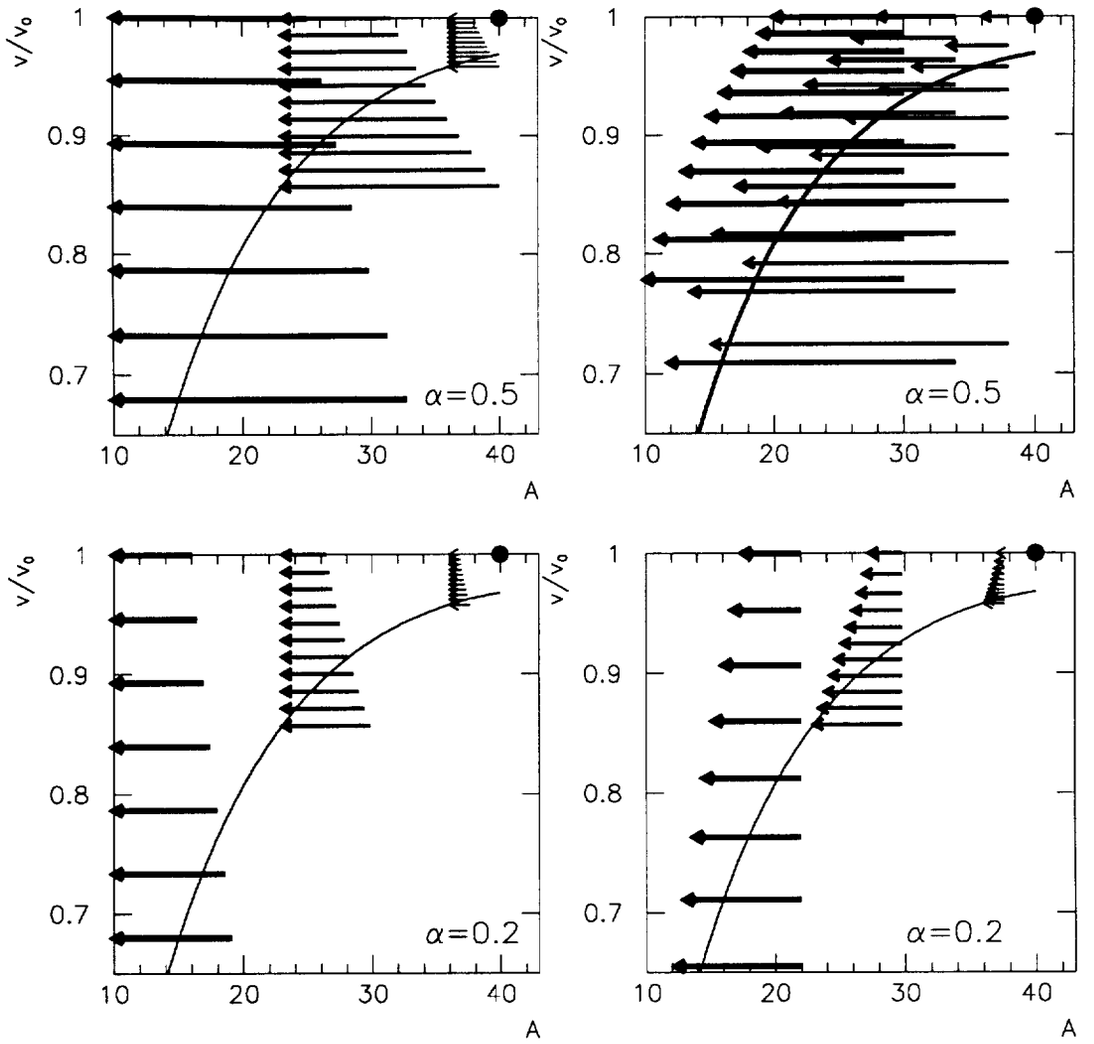

Fig.9 Schematized representation of a sample of two step fragmentation events in the relative velocity versus fragment mass plane. The bold dot is the starting point, the projectile with A=40 and V/V_0=1. The first (fast) step leads to the arrow tails while the second (evaporation) step from the tail to the head (horizontal arrow, no velocity change). Two values of α_0 are presented. On the top half of the figure, α_0 has its upper bound $\alpha_0 = \alpha_{0\,max}$=0.5 whereas on the bottom half, a smaller value α_0 =0.2 has been chosen. On the left half of the figure, A_F is kept constant (3 values at 10, 23 and 36) whereas the intermediate fragment mass A_I is kept constant on the right hand part of the figure (3 values at 30, 34 and 38 for α_0 =0.5, and 3 values at 22, 30 and 38 for α_0 =0.2). The line $v_{1/10}(A_F)$ locates events of a given final mass A_F where the yield has gone down by a factor of 10.

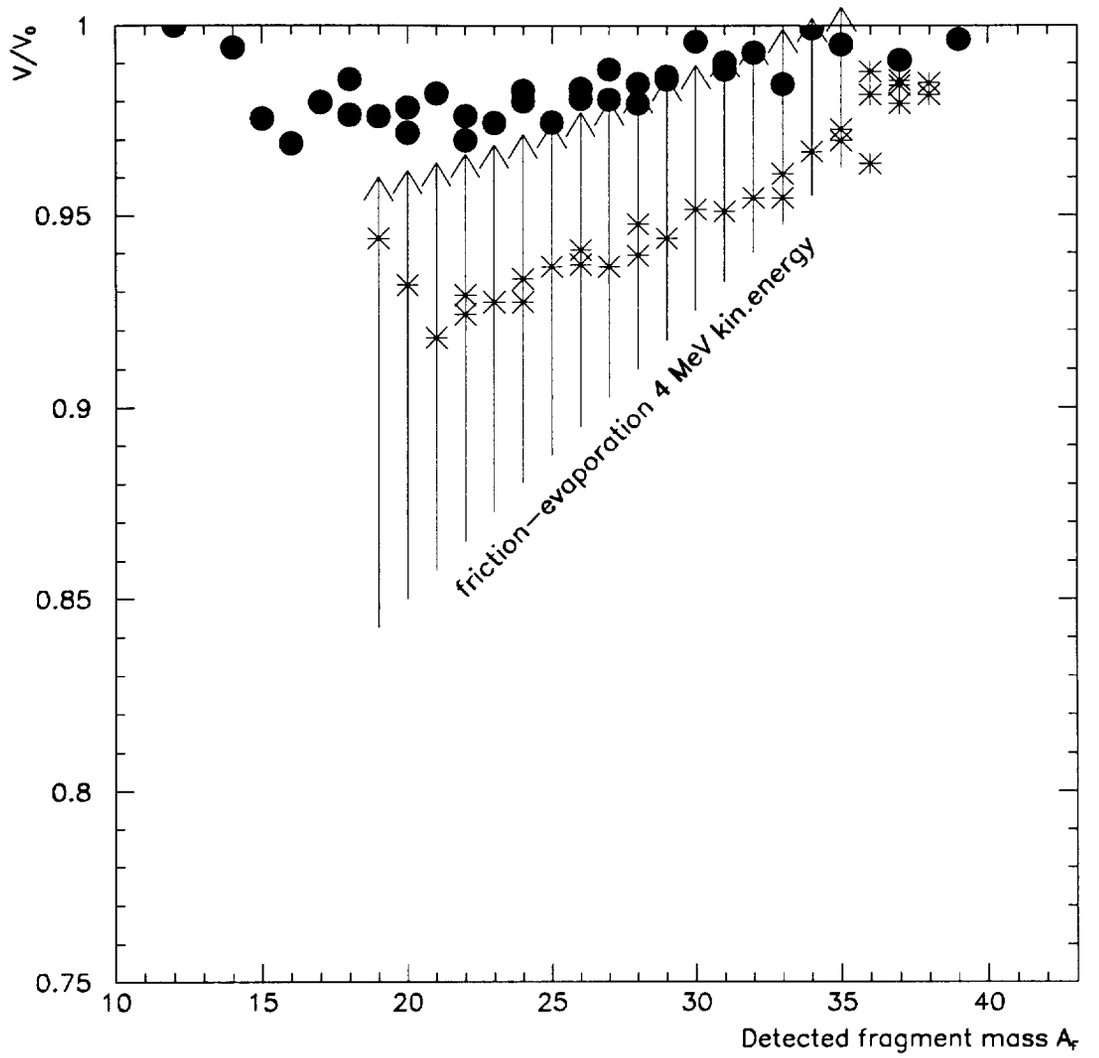

Fig.10 Same plot as in Fig.1. The most probable velocity for the forward (bold points) and grazing angle (stars) fragments are compared to a friction evaporation model with a "velocity gain" equal to the Gaussian width calculated from the Goldhaber scheme with σ_0=100 MeV/c.